JOURNAL OF MATERIALS SCIENCE 32 (1997) 4661–4671

Preparation and properties of $Pb_{0.99}Nb_{0.02}(Zr_{0.52}Ti_{0.48})_{0.98}O_3$ by a new sol–gel technique

XIAOMING YANG, T. K. CHAKI*
Department of Mechanical and Aerospace Engineering, State University of New York, Buffalo, NY 14260, USA

A new sol–gel processing technique has been developed for preparing Nb-doped lead zirconate titanate (PZT) with the composition $Pb_{0.99}Nb_{0.02}(Zr_{0.52}Ti_{0.48})_{0.98}O_3$. The sol was prepared from $Pb(NO_3)_2$, $NbCl_5$, $Ti(OC_3H_7)_4$ and $Zr(C_4H_9O)_4$, dissolved in *N*, *N*-dimethylformamide with stirring at ambient atmosphere. The gel was calcined at 500 °C for 30 min and pressed pellets were sintered in air at 1000 °C for 2–20 h. The average grain size in the pellets sintered for 4 h was about 1.4 μm, which was smaller than that in undoped PZT pellets. Nb doping decreased angle α in the rhombohedral crystal structure, thereby enhancing electromechanical coupling.

1. Introduction

Lead zirconate titanate (PZT) [1] is a ferroelectric ceramic, widely used as a piezoelectric material in many sensor and actuator applications [2, 3] because of its large electromechanical coupling coefficients, ease of fabrication, temperature stability, and high resistance to depolarization. Near the morphotropic phase boundary between the tetragonal and the rhombohedral (ferroelectric) phases in the binary $PbZrO_3$–$PbTiO_3$ system (at 50–55 mol % $PbZrO_3$), the dielectric constant and the electromechanical coupling coefficients show maximum values [1]. Consequently, commercial PZT is usually prepared with a composition near the morphotropic boundary. To enhance the properties of PZT further, various dopants, such as Nb, La, Fe, Sb, Ta, Cr, Co or Mn, are added [1, 4]. An addition of small quantities of pentavalent element Nb^{5+} (donor type) produces Pb vacancies (A-vacancy in ABO_3 perovskite) in PZT and enhances domain reorientation [5], resulting in square hysteresis loops, low coercivity, high remanent polarization, high dielectric constant, high electromechanical coupling factors, high dielectric loss, high compliance, and reduced aging. Nb-doped PZT (called PNZT) is used in high-sensitivity devices, such as hydrophones, phonograph pickups, sounders, and loudspeakers. Furthermore, Nb-doping reduces the temperature dependency of piezoelectric constants [6].

In conventional processing [6, 7] PZT and PNZT are prepared by calcining PbO, ZrO_2, TiO_2 and Nb_2O_5 powders at about 900 °C for a few hours and then sintering in air at 1200–1300 °C for 2–4 h. In recent years sol–gel processing [8] has become popular for producing ceramic materials with improved compositional homogeneity and lower sintering temperatures. PZT powder and thick films have been prepared by various sol–gel routes, starting from different metallo-organic materials. Higuchi *et al.* [9] prepared sol–gel derived PZT films by dissolving zirconium tetra-*n*-propoxide, lead acetate trihydrate and titanium tetra-isopropoxide in isopropyl alcohol, and reported persistence presence of fine pyrochlore grains even after annealing at 600 °C for 1 h in air. Aoki *et al.* [10] prepared PZT films from a gel derived by dissolving lead acetate trihydrate, titanium i-propoxide and zirconium i-propoxide in methoxyethanol, and subsequently annealed the films at 600 °C for 1 h in air. Yi *et al.* [11] prepared PZT films from a sol, which was stable under ambient conditions, with lead acetate trihydrate, zirconium propoxide and titanium isopropoxide as the starting materials, and glacial acetic acid and distilled water or propanol as solvents. Obhi and Patel [12] prepared PZT films by a sol–gel route, in which a mixture of titanium (IV) butoxide and zirconium (IV) butoxide butanol was reacted with 2-methoxyethanol under reflux for 2 h in dry N_2. Lead (II) acetate trihydrate was reacted with 2-methoxyethanol under reflux for 2 h. Then the Ti–Zr precursor and the Pb precursor were mixed and refluxed for 1 h under dry N_2. Butyl acetate was removed by distillation and the resulting solution was the PZT sol. Using this method, Obhi and Patel [12] obtained films of PZT phase by annealing at 450 °C

* To whom correspondence should be addressed.

0022–2461

for 30 min. Lakeman and Payne [13] critically examined the formation of PZT dried gel, powder and films from an acetate-alkoxide solution with reflux and distillation (a method similar to that used by Obhi and Patel [12]), and observed that the precursor solution was sensitive to handling and processing conditions, such that single-phase, perovskite PZT was obtained only with suitable control of the processing parameters.

Only a few reports of preparation of PNZT (Nb-doped PZT) by sol–gel routes are available. Barlingay and Dey [14] fabricated PNZT films from a sol prepared by reacting Ti and Zr-methoxyethoxide with anhydrous Pb-acetate under dry N_2. Niobium methoxyethoxide was added in required quantity as the Nb precursor. Carim *et al.* [15] used lead 2-ethylhexanoate, zirconium tetra-*n*-butoxide, and titanium tetra-isopropoxide to prepare the precursor solution, and niobium penta-ethoxide was introduced for Nb doping. Using this sol, Carim *et al.* [15] deposited PNZT films by annealing at 650 °C for 30 min. Many of the methods described above for preparing PZT and PNZT involve expensive metallo-organic compounds, which are often sensitive to air, and consequently the sol has to be maintained under an inert atmosphere. Phule [16] has molecularly modified transition metal alkoxides for enhancing stability. Here we describe a new sol–gel method for preparing PNZT powder, starting from commonly available chemicals, which are stable in ambient atmosphere. Wherever possible, inorganic compounds have been used. We have also examined the effects of Nb doping upon the microstructure and piezoelectric properties of PZT.

2. Experimental methods

A sol for PNZT was prepared from the following starting chemicals: lead nitrate [$Pb(NO_3)_2$], niobium pentachloride [$NbCl_5$], zirconium *n*-butoxide [$Zr(C_4H_9O)_4$] and titanium isopropoxide [$Ti(OC_3H_7)_4$], taken in amounts of the cation ratio in the chemical formula $Pb_xNb_{0.02}(Zr_{0.52}Ti_{0.48})_{0.98}O_3$. For maintainance of charge neutrality [1] upon addition of pentavalent Nb, x should be 0.99. However, to compensate Pb loss during subsequent firing of the gel, we added excess lead and took the initial x to be 1.2. All the starting chemicals were of ACS grade and no attempt was made for removal of any chlorine impurity. First, $Pb(NO_3)_2$ was dissolved in anhydrous *N*, *N*-dimethylformamide (DMF) with stirring for 15–20 min in ambient atmosphere. Then, $Zr(C_4H_9O)_4$ and $Ti(OC_3H_7)_4$ liquids were poured into the $Pb(NO_3)_2$/DMF solution and stirred for 45–60 min in ambient atmosphere. Finally, $NbCl_5$ powder was added and the solution was stirred for 10–15 min. The resulting PNZT sol was gelled by an addition of NH_3 aqueous solution. The gel was dried in ambient atmosphere. For comparison, undoped PZT [$Pb_x(Zr_{0.52}Ti_{0.48})O_3$] gel was prepared using the same procedure. The initial value of x (Pb atom fraction) in PZT was taken as 1.2 (after a few trials with other values of x).

The dried gel was calcined at 500 °C in air for 30 min. Heating from room temperature to 500 °C took about 3 h. The calcined mass was ground to a fine powder, the particle size of which was analysed by Brunauer–Emmett–Teller (BET) nitrogen adsorption. About 1 mm thick pellets were prepared by compacting the powder inside a cylindrical die of inner diameter 12.7 mm under a stress of 350 MPa and then sintering at 1000 °C in air inside an open-ended tube furnace of 75 cm length and 7.5 cm inner diameter. The duration of sintering was varied between 2 and 20 h to optimize the piezoelectric properties of the pellets. X-ray diffraction methods with CuK_α radiation were used to characterize the phases in the pellets. Differential thermal analysis (DTA; Perkin Elmer DTA7) and thermogravimetric analysis (TGA; Perkin Elmer TGA 7HT) of the gel were performed in flowing air from room temperature to 1050 °C at a heating rate of 20 °C min^{-1}. Scanning electron microscopy (SEM) was used to examine the microstructure on the surface of the pellets sintered for various periods of time. The grain size was measured by the linear intercept method from the SEM micrographs. A few pellets were broken perpendicular to the flat surface, and the fracture surface was examined by SEM. The density of the pellets was determined by measuring the mass and volume of the pellets. The volume of the pellet was measured by the liquid displacement method using water. The hardness of the pellet was measured by Vickers indentation under a load of 200 g. The value of the microhardness was calculated using $H = 1.8544P/d^2$ kg mm^{-2}, where P is the applied load in kg and d is the diagonal length of the impression in mm.

For evaluation of piezoelectric properties, a layer of silver paint was applied on each of the flat surfaces of the pellet and dried in air at room temperature. The pellet was placed inside two copper plates in a spring-loaded jig. The Cu plates firmly touched the Ag painted area, and were used as electrode connections. The pellet was poled inside silicone oil maintained at 90 °C under an electric field of 4 kV mm^{-1} for 30 min. The dielectric constant (K_{33}^{T}) of the poled pellet was estimated by measuring the capacitance on an LCR meter (BK Precision, model 875A) at low frequency (1 kHz). The planar coupling factor (k_p) was determined by measuring the resonant and antiresonant frequencies of the poled pellet, following the IRE (Institute of Radio Engineers) Standards [17]. k_p was calculated by using the relation [18]

$$k_p^2 = 1 - \frac{f_r^2}{f_a^2} \quad (1)$$

where f_r and f_a are resonant and antiresonant frequencies, respectively. A few rectangular bars of size 13.5 mm × 5.5 mm × 0.5 mm were prepared by compacting calcined powder and firing in air at 1000 °C for 4 h. The opposite surfaces with the largest area were coated with Ag paint and dried in air. On one surface a 120-ohm strain gauge was attached by M200 bond for measuring strains along the length of the bar. M200 bond provided electrical insulation between the strain gauge and the silver paint, which was grounded to zero potential. The silver paint on the other surface

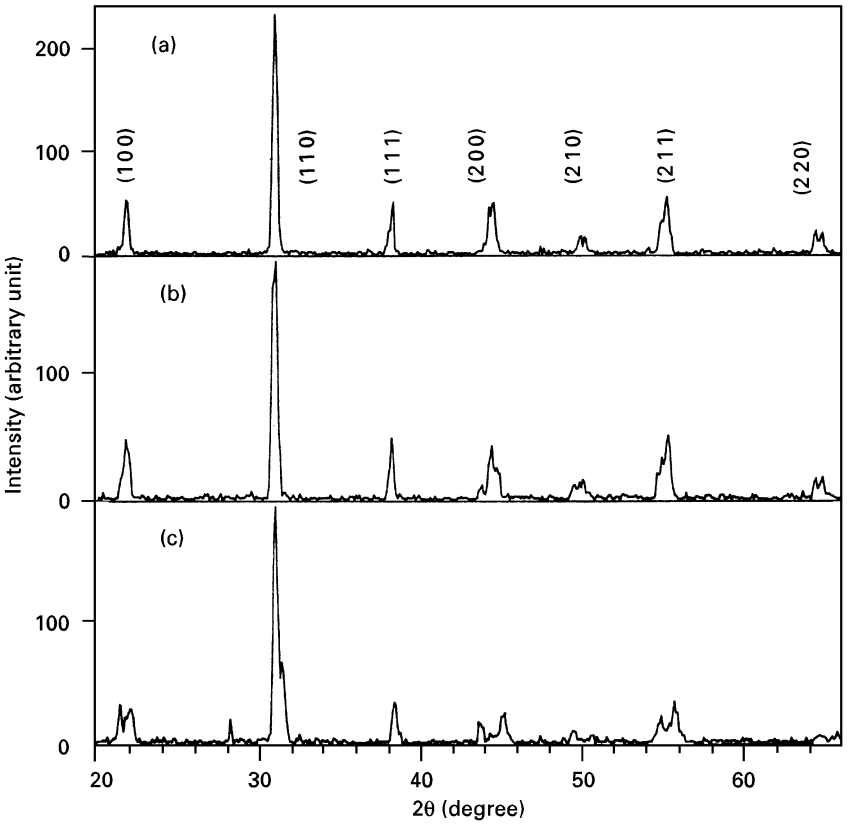

Figure 1 X-ray diffraction patterns of PZT pellets with various initial Pb contents upon sintering in air at 1000 °C for 2 h. (a) 1.2; (b) 1.1; and (c) 1.0 atom fraction.

was connected to the positive terminal of a high voltage power supply. The specimen with strain gauge was dipped into silicone oil at room temperature. As the voltage was applied, the strain was recorded using a computerized data acquisition system.

3. Results and discussion

3.1. X-ray diffraction

Fig. 1a, b and c show X-ray diffraction patterns (in reflection mode) of undoped PZT pellets with initial Pb contents of 1.2, 1.1 and 1.0 atom fractions, respectively. All the pellets were sintered at 1000 °C in air for 2 h. At the initial Pb content of 1.2 atom fraction, the sintered pellets contained pure perovskite phase, as indicated by the sharp peaks in the X-ray diffraction pattern (Fig. 1a). At 1.0 atom fraction of the initial Pb content the X-ray diffraction peaks became distorted with some splitting (Fig. 1c), possibly due to the presence of Pb-deficient perovskite phase. The initial Pb content affected the lattice parameters in the rhombohedral crystal structure, a schematic of which is shown in Fig. 2. The lattice parameters (edge length, a, and rhombohedral angle, α) decreased with the increasing Pb content (Table I). At the initial lead content of 1.2, α in PZT pellets, sintered at 1000 °C for 2 h in air, was 89.94 degrees, which was slightly less than 90 degrees, thereby producing rhombohedral distortion. All subsequent pellets of both PZT and PNZT were prepared with an initial Pb content of 1.2 atom fraction. However, there is a difference in the final Pb contents of the two materials. In PZT the desired composition is $Pb(Zr_{0.52}Ti_{0.48})O_3$, while that in

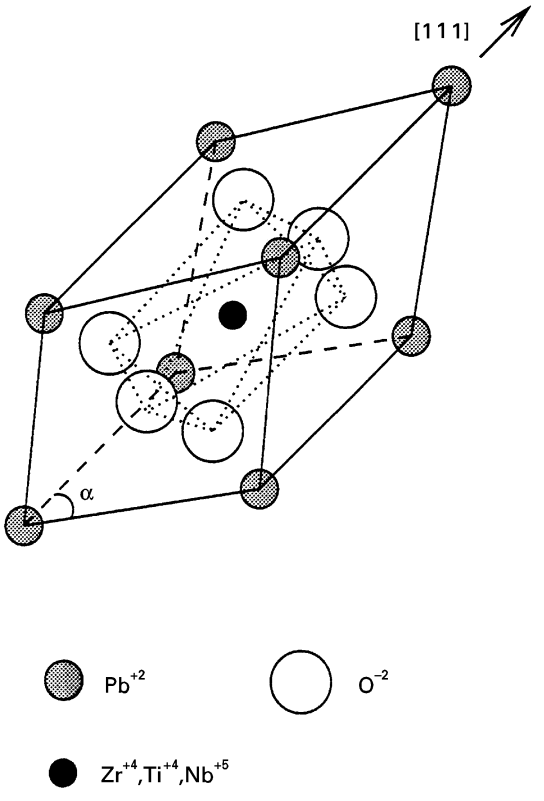

Figure 2 A schematic of the rhombohedral crystal structure of PZT.

PNZT, as required by charge neutrality, is $Pb_{0.99}Nb_{0.02}(Zr_{0.52}Ti_{0.48})O_3$. Thus, with the initial Pb content of 1.2 atom fraction, PZT and PNZT pellets had to lose during sintering 0.2 and 0.21 atom

fractions of Pb, respectively. The sintering time can affect Pb loss. In later sections we will discuss the effects of the sintering duration on various properties of PZT and PNZT pellets.

Fig. 3a, b and c show X-ray diffraction patterns of PZT pellets sintered in air for 2 h at 1000, 950 and 500 °C, respectively. All the pellets had an initial Pb content of 1.2 atom fraction. Upon firing at 500 °C, the reactions were not complete [1] and the material contained some amount of $PbTiO_3$. Upon sintering at 950 °C, no peak other than those of the PZT perovskite phase was observed (Fig. 3b). Fig. 4a, b and c show X-ray diffraction patterns of PNZT pellets sintered in air for 2 h at 1000, 950 and 500 °C, respectively. All the PNZT pellets had an initial Pb content of 1.2 atom fraction. Again, the reactions were not complete at 500°C and some $Pb_2Nb_2TiO_9$ phase was present in PNZT fired at 500°C (Fig. 4c). Upon sintering PNZT at 950°C, most of the unwanted phases disappeared (Fig. 4b). PNZT sintered at 1000°C contained the pure perovskite phase, as seen by the sharp peaks in the X-ray diffraction pattern (Fig. 4a). It should be noted that PZT and PNZT prepared by the present sol–gel method did not contain any pyrochlore phase upon calcining at 500°C, compared with some other sol–gel routes [9, 13] in which pyrochlore was present even after firing at 650°C. Even though the X-ray diffraction patterns upon sintering at 950 and 1000°C (for both PZT and PNZT) looked similar, there were subtle differences, as illustrated in Table II, which tabulates the lattice parameters (a and α) of PZT and PNZT sintered at various temperatures. The values of α for PZT and PNZT pellets sintered at 950°C were 90.14 and 90.52 degrees, respectively. However, upon sintering at 1000°C the values of α for PZT and PNZT were 89.94 and 88.73 degrees, respectively, which were less than 90 degrees, thereby producing rhombohedral elongation along [1 1 1] direction. The rhombohedral distortion in PNZT sintered at 1000°C was 90–88.73 = 1.27 degree, which was larger than that (90–89.94 = 0.06 degree) in PZT. Nb^{5+} ions substituted [5] Zr^{4+} or Ti^{4+} in the centre of the PZT lattice (Fig. 2) and caused a large distortion of the lattice. A larger rhombohedral distortion in PNZT enhanced piezoelectric properties, which will be discussed in a later section.

TABLE I Lattice parameters of PZT sintered at 1000 °C for 2 h in air

Initial Pb Content (atom fraction)	a (nm)	α (degree)
1.0	0.4176	92.32
1.1	0.4088	90.45
1.2	0.4088	89.94

3.2. Thermal analysis

Fig. 5a shows DTA and TGA of PZT gel samples of weight 13.280 and 11.447 mg, respectively. When a peak in the DTA curve occurred, the onset temperature of the process was taken at the point where a horizontal tangent before the increase in the temperature differential (ΔT) intersected with the tangent at the region of steady increase in ΔT, and the finish

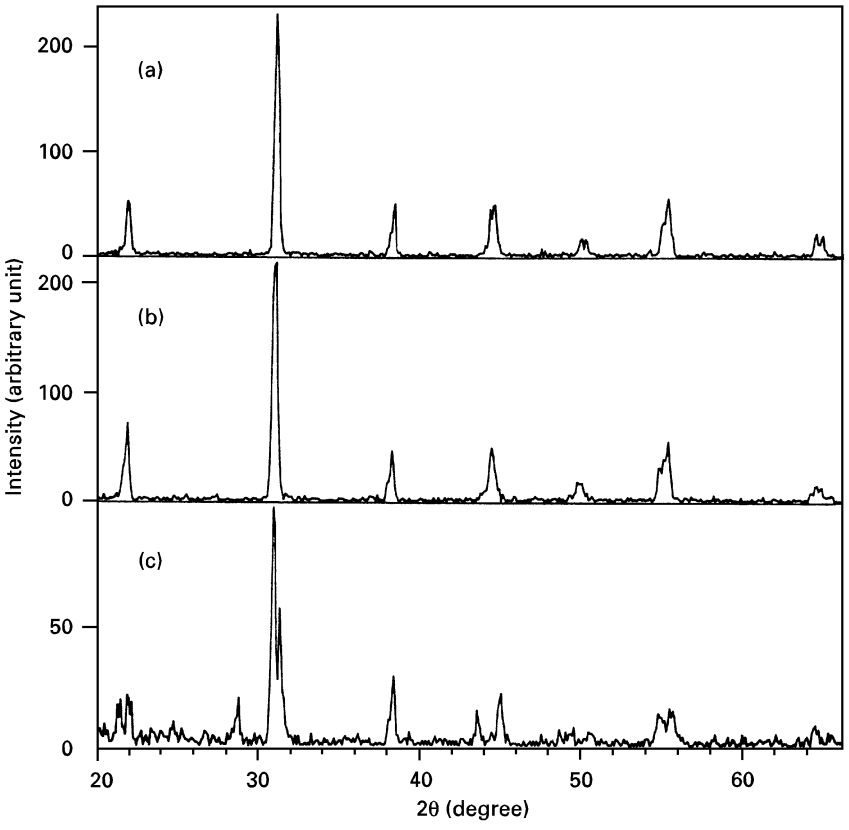

Figure 3 X-ray diffraction patterns of PZT pellets sintered in air for 2 h at various temperatures. (a) 1000 °C; (b) 950 °C; and (c) 500 °C.

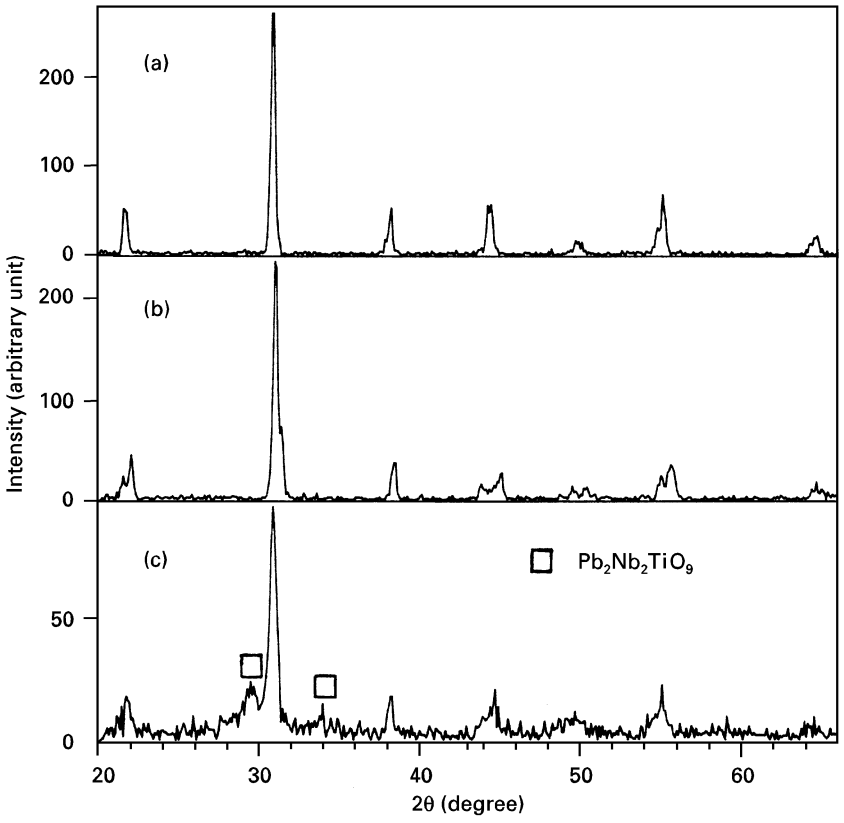

Figure 4 X-ray diffraction patterns of PNZT pellets sintered in air for 2 h at various temperatures. (a) 1000 °C; (b) 950 °C; and (c) 500 °C.

TABLE II Lattice parameters of PZT and PNZT with 1.2 atom fraction of initial Pb content. Sintering was done for 2 h in air

Sintering temperature (°C)	PZT		PNZT	
	a (nm)	α (degree)	*a* (nm)	α (degree)
500	0.4088	89.47	0.4088	89.94
950	0.4077	90.14	0.4126	90.52
1000	0.4088	89.94	0.4029	88.73

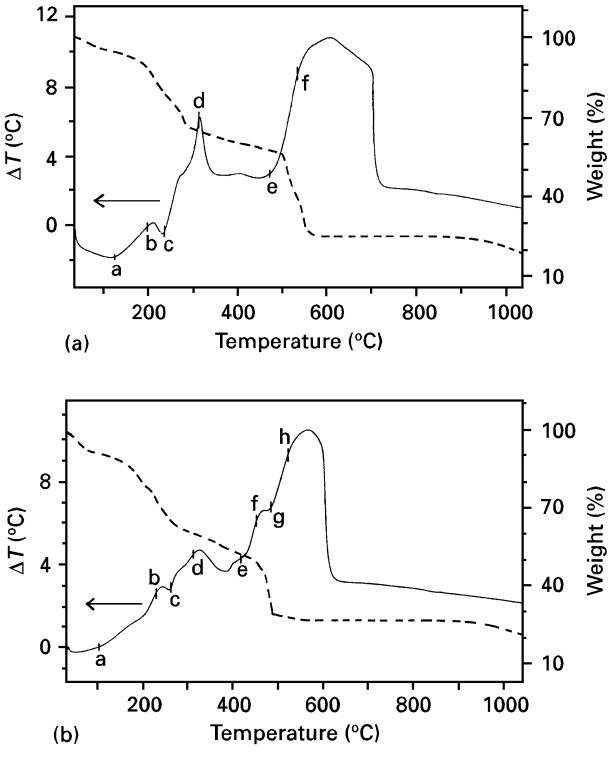

Figure 5 DTA and TGA results. (a) PZT; and (b) PNZT.

temperature was taken at the point where the slope in the ΔT–T curve started to decrease. In the DTA curve (Fig. 5a) segments of "ab" and "cd" were attributed to dehydration and decomposition of organic precursors, respectively. Both these processes were accompanied by weight loss. Segment "ef" (from 480 to 540 °C) corresponded to an exothermic transformation to the perovskite PZT phase. This transformation was accompanied by a rapid weight loss. It is likely that the remaining organic species decomposed in this temperature range. In the sol–gel method of Lakeman and Payne [13] the major exotherm in the DTA of the PZT gel occurred around 500–600 °C, and there were several smaller peaks at higher temperatures, with completion of all reactions at 800 °C. In our sol–gel method all reactions in the PZT gel were complete at 540 °C, which was smaller than the temperature in Lakeman and Payne's method [13].

Fig. 5b shows DTA and TGA of PNZT gel samples of weight 8.040 and 7.517 mg, respectively. The thermal analysis curves for PNZT were similar to those of PZT. In the DTA curve of PNZT gel (Fig. 5b) segments "ab" and "cd" were attributed to dehydration and decomposition of organic precursors, respectively, and occurred in similar temperature ranges as those in PZT. Segment "efgh" corresponded to the transformation

to the perovskite phase of PNZT. The horizontal part (segment "fg") was probably due to the presence of two species bound differently in the PNZT gel. The transformation of one species (indicated by segment "gh") occurred in the temperature range 480–540°C, which is the same as the transformation temperature range in undoped PZT. The other species in PNZT transformed (indicated by segment "ef") at lower temperatures (415–450 °C).

3.3. Microstructure

The morphologies of the PZT and PNZT dried gels were similar, as shown in Fig. 6a and b. The particles in the dried gels were interconnected and agglomerated. The agglomeration probably depended on the initial choice of the organic liquids. The powders of PZT and PNZT, obtained upon calcination and grinding, had surface areas of 4.2 and 5.1 $m^2 g^{-1}$. The microstructure of PZT pellets is shown in Fig. 7a, b and c. The grain structure on the flat surface of a PZT pellet sintered at 1000 °C for 4 h is shown in Fig. 7a. There was grooving at the grain boundaries. Fig. 7b shows the fracture surface of a PZT pellet sintered at 1000 °C for 4 h. The fracture was transgranular, with river patterns on the fracture surface. The pores are also seen on the fracture surface. Fig. 7c shows the fracture surface of a PZT pellet sintered at 1000 °C for 2 h. Here the fracture was predominantly transgranular with some areas of intergranular fracture. The presence of some particles due to intergranular fracture could be seen (Fig. 7c), because 2 h of sintering was probably not enough for the development of strong bonding among all the particles.

The microstructure of the PNZT pellets is shown in Fig. 8a, b and c. The grain structure on the surface of a PNZT pellet sintered at 1000 °C for 4 h is shown in Fig. 8a, and the grain size was 1.42 ± 0.07 μm, compared to a value of 4.84 ± 0.23 μm for undoped PZT pellets sintered identically. A comparison of grain sizes in PZT and PNZT pellets sintered at 1000 °C for various periods of sintering time is illustrated in Fig. 9. The grain sizes in the PNZT pellets at all sintering durations were smaller than the corresponding grain sizes in the PZT pellets. There was a linear grain growth in the PZT pellets with sintering time, reaching a grain size of 11.3 ± 0.7 μm after 20 h at 1000°C. In PNZT, after an initial growth, the grains did not grow much with time, reaching only 2.6 ± 0.4 μm in 20 h (Table III). Thus, Nb doping inhibited grain growth. Similar inhibition of grain growth in PZT by dopants has been reported by Hahn and Kostorz [19].

Fig. 8b shows the fracture surface of a PNZT pellet sintered at 1000 °C for 4 h. The fracture was predominantly transgranular. On the other hand, when sintering was done for 2 h at 1000 °C, the fracture of the PNZT pellets was intergranular, as shown in Fig. 8c. In fact, there was little densification of PNZT upon 2 h of sintering at 1000 °C, and the fracture occurred at the neck between the particles. The green density of the PNZT compacts was 4.50 ± 0.57 g cm^{-3}, while the density upon 2 h of sintering at 1000 °C was

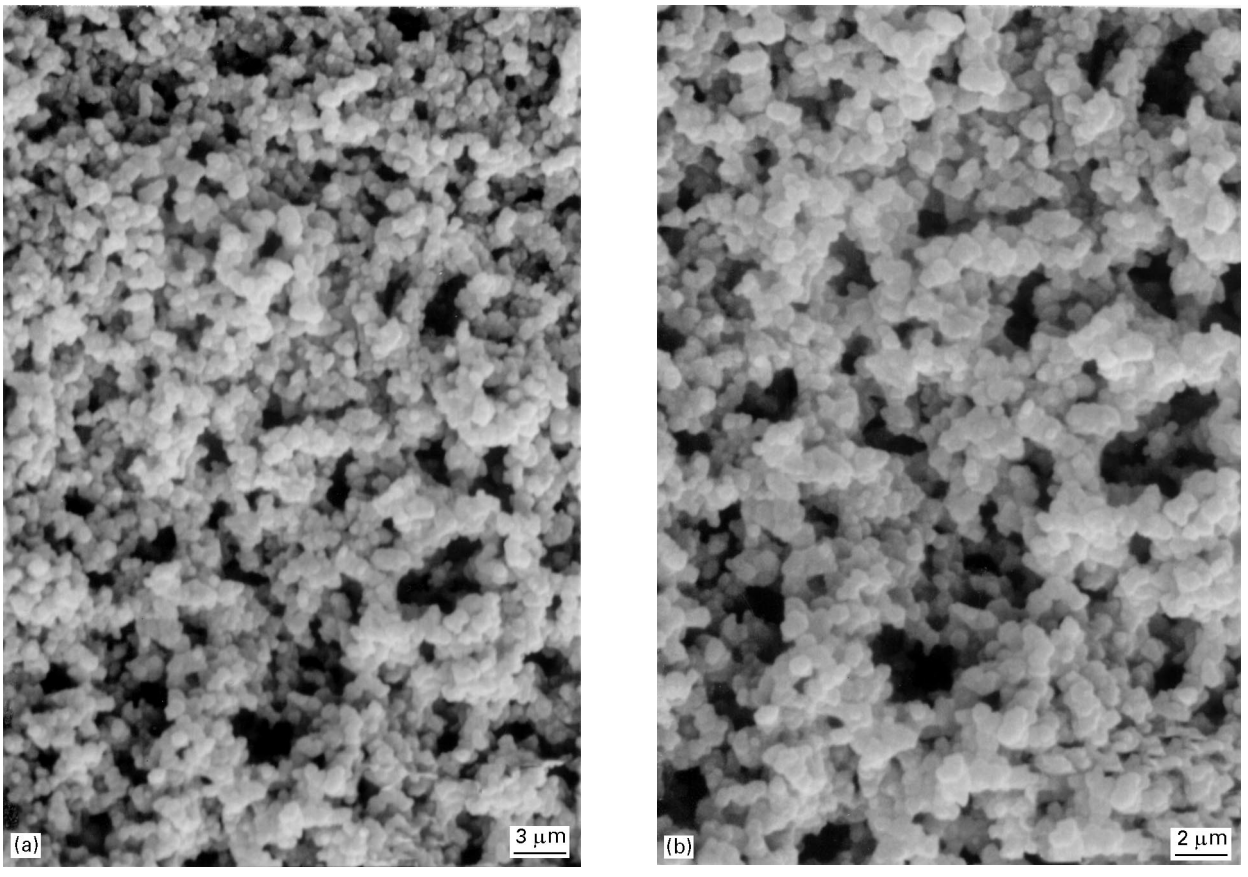

Figure 6 Morphology of the dried gel. (a) PZT; and (b) PNZT.

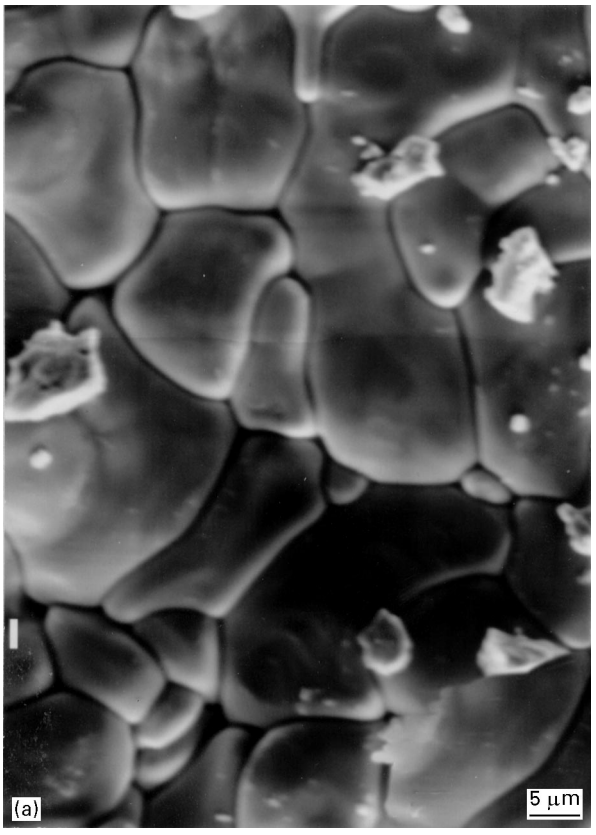

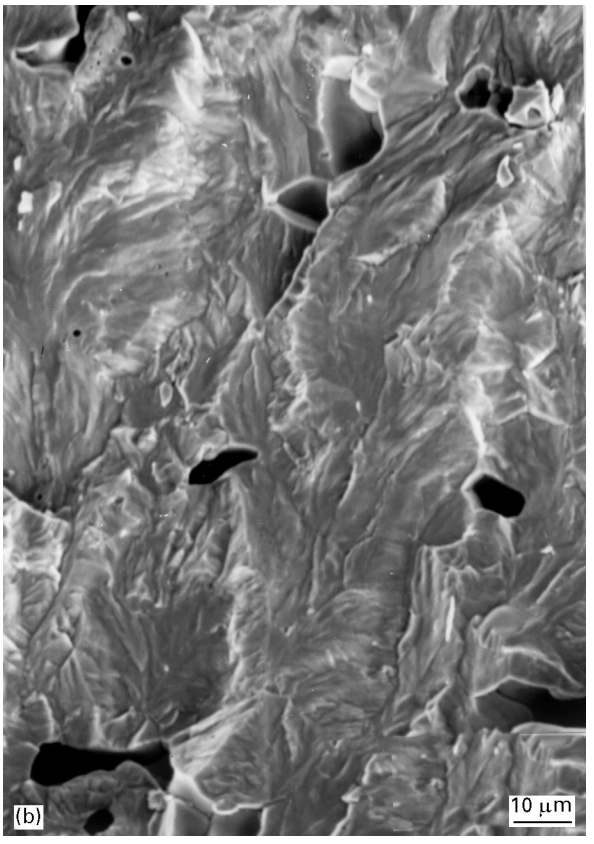

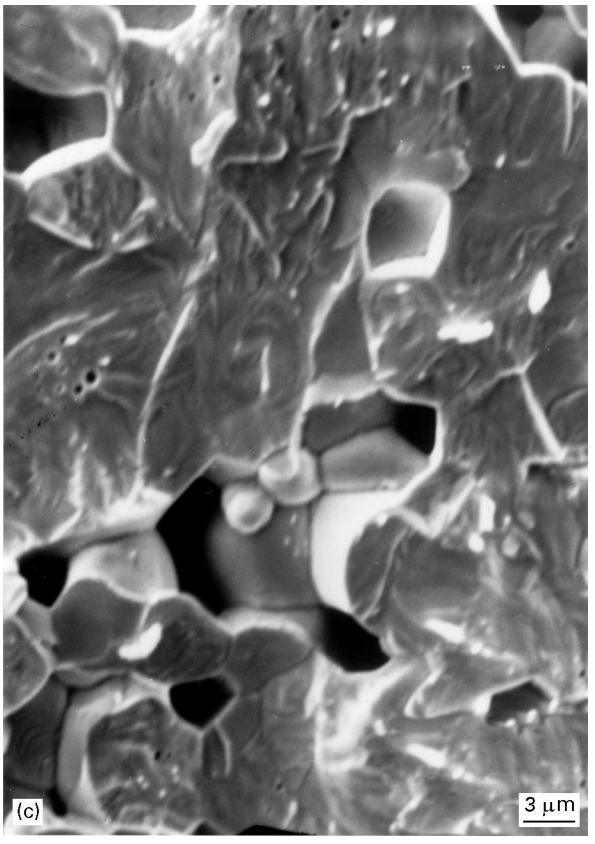

Figure 7 Scanning electron micrographs of PZT pellets. (a) Top surface upon sintering at 1000 °C for 4 h; (b) fracture surface after sintering at 1000 °C for 4 h; and (c) fracture surface after sintering at 1000 °C for 2 h.

$4.57 \pm 0.36\,g\,cm^{-3}$. In contrast, upon sintering for 2 h at 1000 °C the density of PZT increased from 4.56 ± 0.63 to $6.10 \pm 0.45\,g\,cm^{-3}$. A comparison of densification behaviour of PZT and PNZT upon sintering at 1000 °C is shown in Fig. 10. Even though the densification of PNZT was initially sluggish, the density increased rapidly, reaching a maximum value of $6.26 \pm 0.40\,g\,cm^{-3}$ at 4 h, and subsequently decreased to $5.66 \pm 0.39\,g\,cm^{-3}$ at 20 h. For PZT pellets the density reached a maximum value of $6.71 \pm 0.51\,g\,cm^{-3}$ (about 83% of the theoretical density) at 6 h and then decreased to $6.05 \pm 0.49\,g\,cm^{-3}$ at 20 h. The sluggish densification of PNZT in the first 2 h of sintering at 1000 °C was probably due to the presence of Nb-rich, unwanted phases (such as $Pb_2Nb_2TiO_9$), which transformed slowly at the sintering temperature. The decrease in the densities of both PZT and PNZT pellets upon prolonged sintering at 1000 °C may be attributed to excessive Pb loss.

It should be noted that PZT-5, a commercial material developed by Vernitron Division of Morgan Matroc, Inc., has a density of $7.5\,g\,cm^{-3}$ (94% of the theoretical density) [20]. The high density is achieved in the commercially used metal oxide process [4, 21] by pressureless sintering at approximately 1275 °C for several hours. Lead loss is controlled by an addition of excess Pb and by sintering in a PbO-rich atmosphere [7]. Uniaxial hot-pressing [21, 22] for long periods (tens of hours) at lower temperature (~ 1200 °C) can produce PZT pellets close to theoretical density. One obvious reason for low densities of PZT pellets (maximum 83% of theoretical density) obtained in the present study is that the pressureless sintering was done at a relatively low temperature (only 1000 °C) without any control of Pb environment. The present

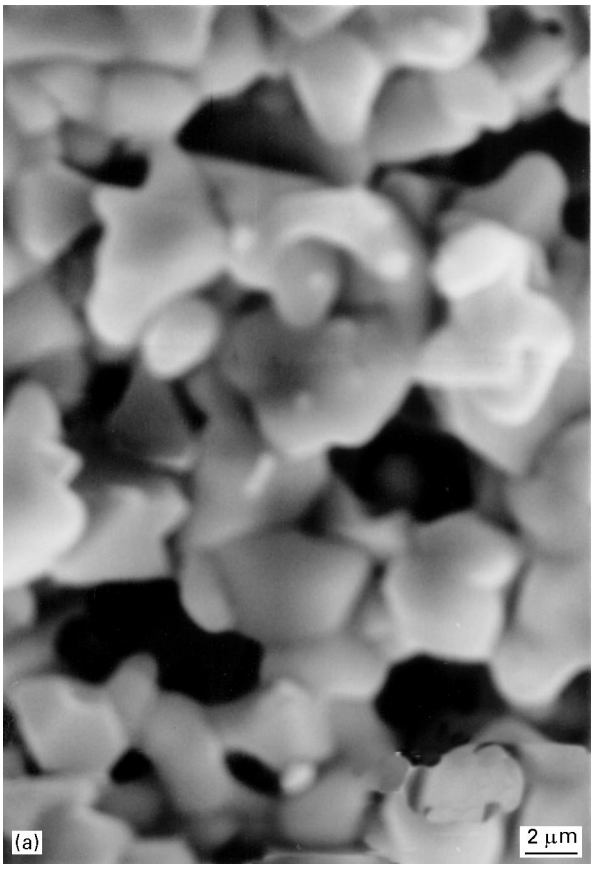

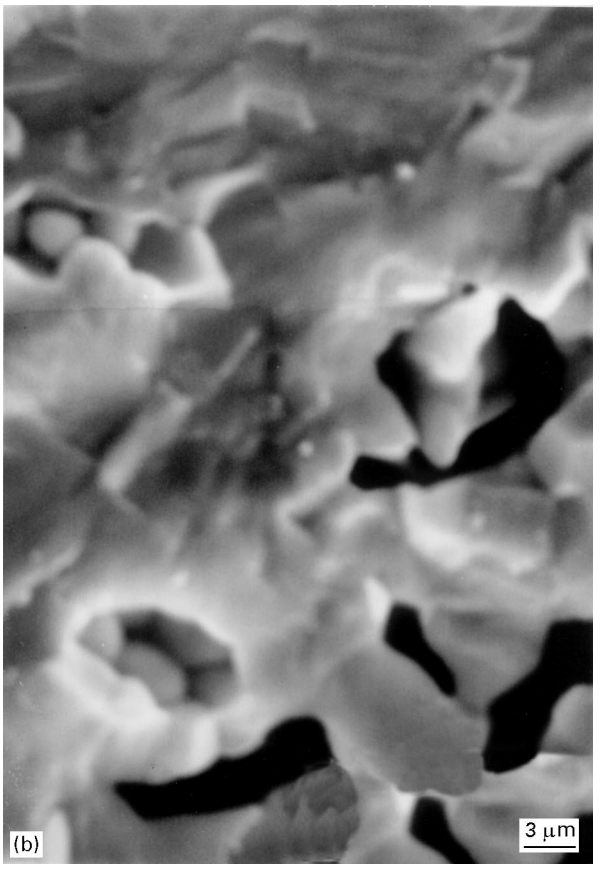

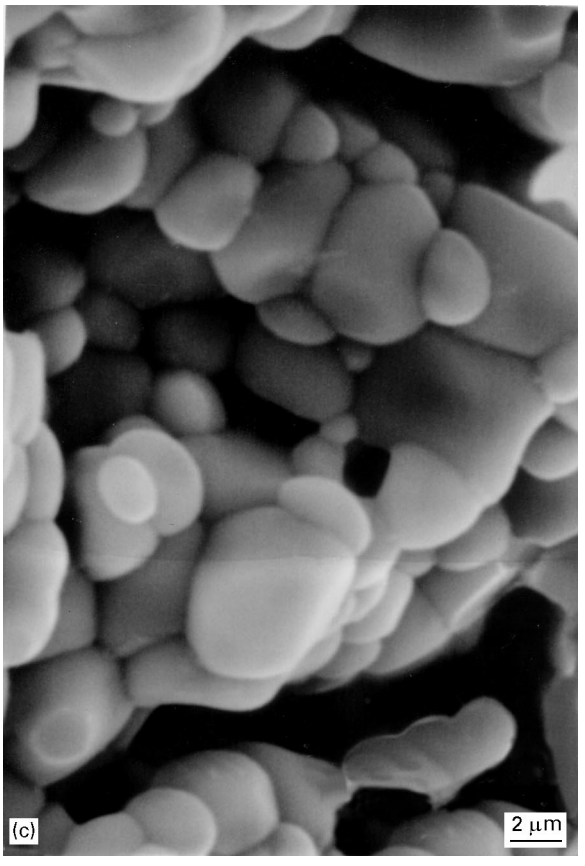

Figure 8 Scanning electron micrographs of PNZT pellets. (a) Top surface upon sintering at 1000 °C for 4 h; (b) fracture surface after sintering at 1000 °C for 4 h; and (c) fracture surface after sintering at 1000 °C for 2 h.

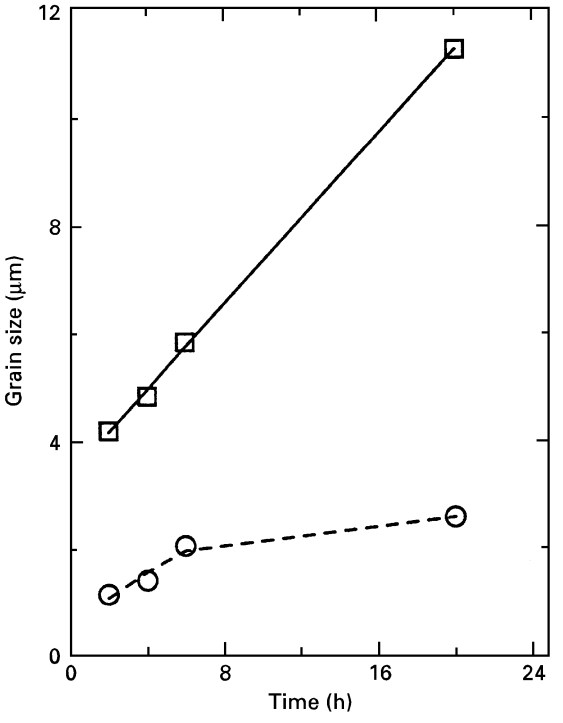

Figure 9 Grain size against sintering time at 1000 °C: □ PZT; ○ PNZT.

investigation was intended to compare the properties of PZT and PNZT. Sinterability to high densities will be studied in the future. The sintering temperature of 1000 °C was selected in this study, because this is the lowest sintering temperature at which the X-ray diffraction pattern became sharp, indicating a high concentration of the perovskite phase.

Even though the densification of PNZT was sluggish at the initial stage of sintering, the Vickers hardness of

TABLE III Properties of PNZT and PZT discs made by sintering at 1000 °C for various periods of time. (Values are mean ± standard deviation, measured over 3 specimens)

Sintering time (h)		2	4	6	20
Grain size (μm)	PNZT	1.16 ± 0.11	1.42 ± 0.07	2.06 ± 0.52	2.59 ± 0.35
	PZT	4.21 ± 0.44	4.84 ± 0.23	5.85 ± 0.36	11.27 ± 0.69
Density ($g\,cm^{-3}$)	PNZT	4.57 ± 0.36	6.26 ± 0.40	5.69 ± 0.48	5.66 ± 0.39
	PZT	6.10 ± 0.45	6.11 ± 0.37	6.71 ± 0.51	6.05 ± 0.49
Vickers hardness ($kg\,mm^{-2}$)	PNZT	287.4 ± 0.3	356.4 ± 0.3	271.0 ± 0.4	120.8 ± 0.1
	PZT	221.5 ± 0.3	308.8 ± 0.6	188.2 ± 0.1	122.0 ± 0.1
Dielectric constant	PNZT	486 ± 32	506 ± 20	625 ± 22	563 ± 42
	PZT	373 ± 15	428 ± 19	491 ± 24	402 ± 20
k_p	PNZT	0.33 ± 0.07	0.47 ± 0.13	0.53 ± 0.21	0.55 ± 0.09
	PZT	0.18 ± 0.03	0.22 ± 0.10	0.31 ± 0.18	0.22 ± 0.03

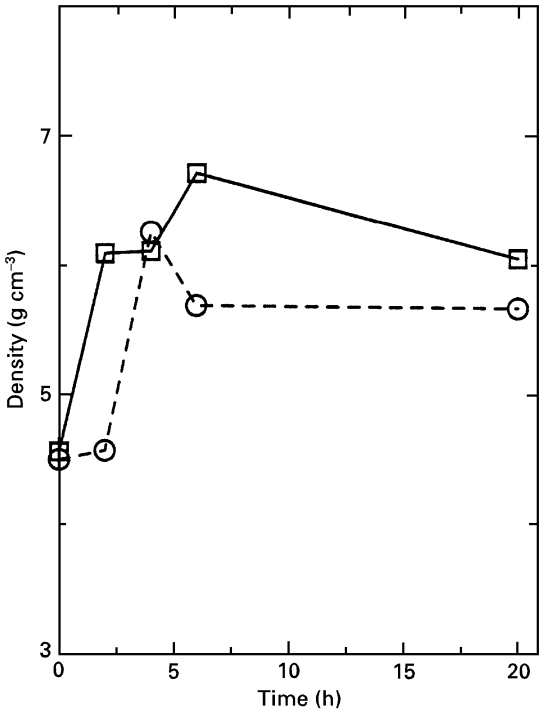

Figure 10 Density against sintering time at 1000 °C: □ PZT; ○ PNZT.

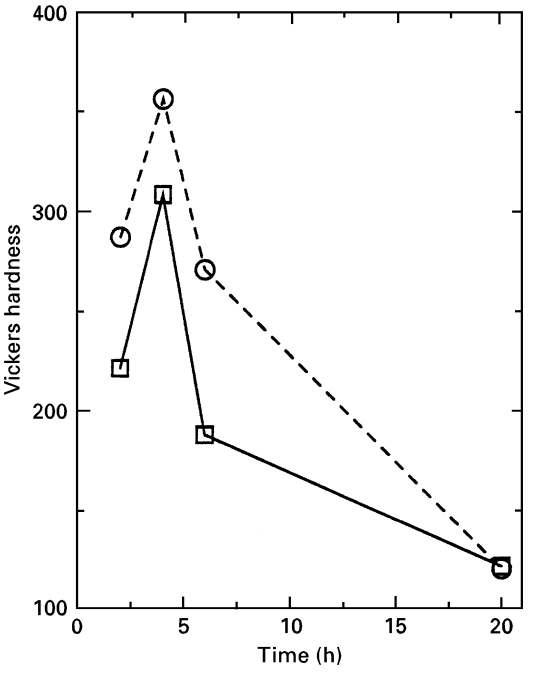

Figure 11 Vickers hardness against sintering time at 1000 °C: □ PZT; ○ PNZT.

the PNZT pellets sintered at 1000 °C for 2 h was 287.4 ± 0.3 $kg\,mm^{-2}$, which was higher than that (221.5 ± 0.3 $kg\,mm^{-2}$) of the PZT pellets sintered identically (Table III). This indicates that in the PNZT pellets with low densities the bonding among the particles was strong, and the PNZT grains were harder than the PZT grains. A comparison of the Vickers hardness values of the PZT and PNZT pellets is shown in Fig. 11. Upon 4 h of sintering at 1000 °C the hardness of the PNZT pellets reached a maximum value of 356.4 ± 0.3 $kg\,mm^{-2}$, which was larger than the maximum hardness (308.8 ± 0.6 $kg\,mm^{-2}$) of the PZT pellets. Thus, Nb doping had a hardening effect in PZT.

3.4. Piezoelectric properties

Fig. 12 shows a plot of the dielectric constant (K_{33}^{T}) of the poled PZT and PNZT pellets against the sintering time at 1000 °C. For both PZT and PNZT the dielectric constant increase with sintering time, reached maximum values, and then decreased. At all durations of sintering the dielectric constant of the PNZT pellets was higher than that of PZT, indicating that Nb doping increased the dielectric constant of PZT. This improvement can be attributed to ease of domain reorientation [5] in PNZT. Another interesting point is that the dielectric constant of the PNZT pellets reached a maximum value of 625 ± 22 upon 6 h of sintering at 1000 °C (Table III), while the density had a maximum value in the pellets sintered for 4 h. Thus, besides the density, some other factor played a role in determining the optimum sintering time. Probably, upon sintering for 6 h, the Pb content in PNZT reached the optimum value (0.99 atom fraction), thereby enhancing the dielectric constant significantly. The decrease in the values of the dielectric constant of both

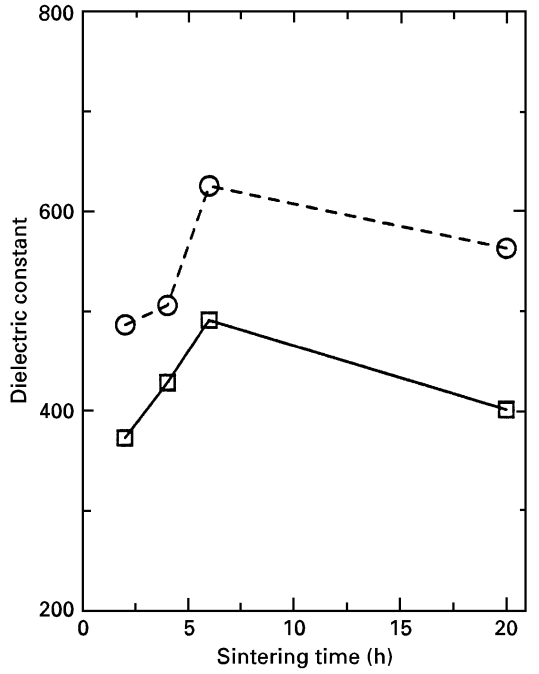

Figure 12 Dielectric constant against sintering time at 1000 °C: □ PZT; ○ PNZT.

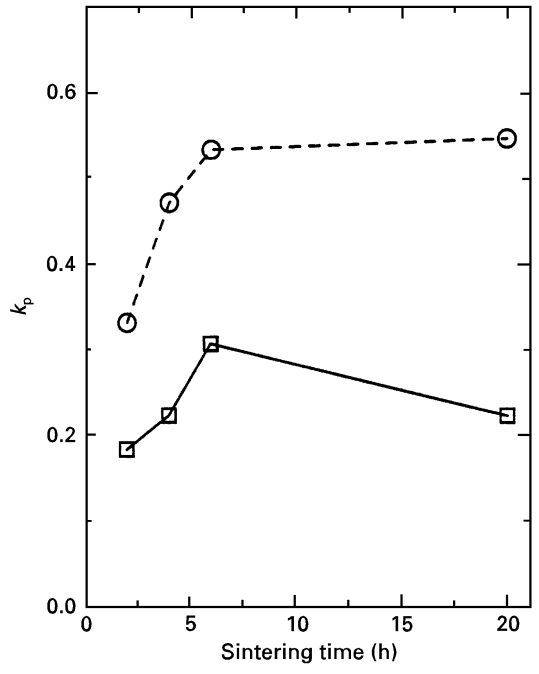

Figure 13 Planar coupling factor (k_p) against sintering time at 1000 °C: □ PZT; ○ PNZT.

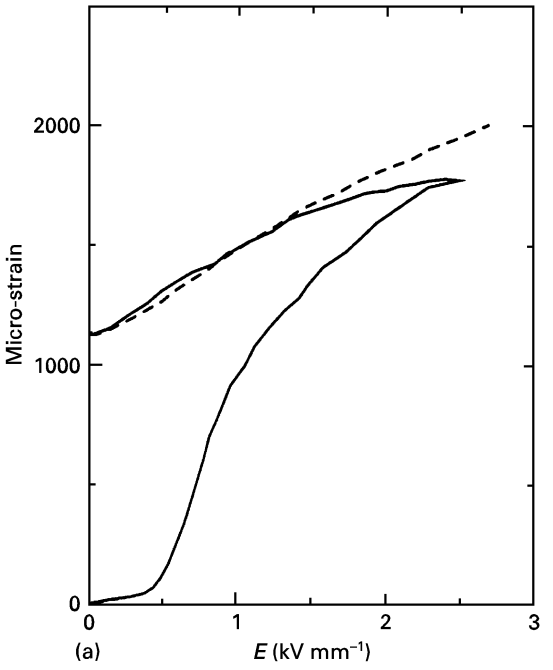

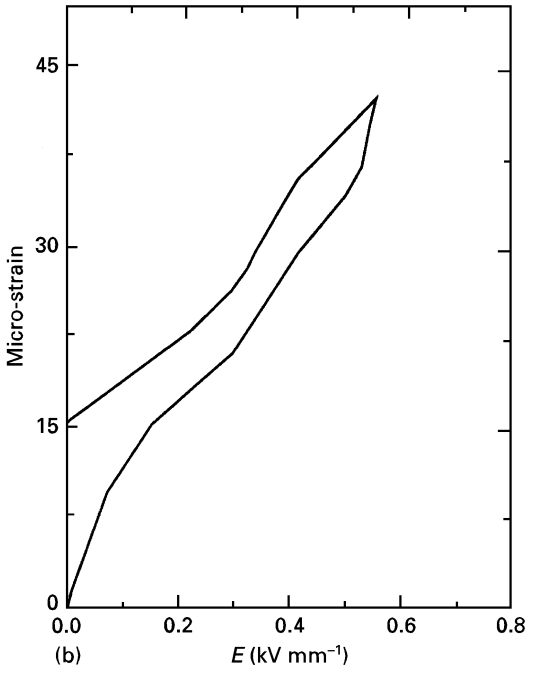

Figure 14 Planar strain against electric field. (a) PNZT; and (b) PZT. The dash line in (a) corresponds to reapplication of the field.

PZT and PNZT upon prolonged sintering may be attributed to excessive Pb losses as well as to the decrease in the densities.

The variation of the planar coupling factor (k_p) of the PZT and PNZT pellets with the sintering time at 1000 °C is shown in Fig. 13. At all sintering durations k_p values of the PNZT pellets were larger than the corresponding k_p values of the PZT pellets. Thus, Nb doping enhanced the planar coupling in PZT. The value of k_p in undoped PZT initially increased with the sintering time, reached a maximum value (0.31 ± 0.18) at 6 h, and then decreased to 0.22 ± 0.03 at 20 h (Table III). In PNZT, however, k_p reached almost a plateau upon 6 h of sintering, and did not decrease even after 20 h of sintering. The maximum value of k_p in PNZT was 0.55 ± 0.09, obtained upon sintering at 1000 °C for 20 h. The variation of k_p with the sintering time might have some correlation with the grain growth. When the sintering time was increased from 6 to 20 h, the grain size of the PNZT pellets increased from 2.06 ± 0.52 μm to only 2.59 ± 0.35 μm, but that of the PZT pellets increased rapidly from 5.85 ± 0.36 to 11.27 ± 0.69 μm. The rapid grain growth during sintering of the undoped PZT pellets might have a deleterious influence on k_p.

The planar strain (measured by a strain gauge) against the electric field is plotted in Fig. 14a and b for PNZT and PZT bars, prepared by sintering at 1000 °C for 4 h. Upon application of an electric field of $2.5\,kV\,mm^{-1}$, the strain in the PNZT bar reached a saturation value (Fig. 14a). The remanent strain in the PNZT bar was about 1125×10^{-6}. Upon reloading, the strain–electric field curve was linear up to about $1\,kV\,mm^{-1}$ and the slope in the linear region was about $-375 \times 10^{-6}\,kV^{-1}\,mm$, which provided an estimate of the strain coefficient (d_{31}) in the PNZT bar. For comparison, the remanent strain in a PZT bar loaded up to about $0.55\,kV\,mm^{-1}$ was 15×10^{-6} and (d_{31}) was $-25 \times 10^{-6}\,kV^{-1}$mm. Thus, Nb doping significantly increased the strain coefficient in PZT and, therefore, can be useful in high-sensitivity piezoelectric devices.

Now we will compare the piezoelectric properties of our sol–gel derived materials with those of PZT-5A [20], a commonly used commercial material. The dielectric constant (K_{33}^{T}) of PZT-5A at room temperature is 1730 at 1 kHz, compared to a maximum value of 625 in our PNZT material. The low value of the dielectric constant in our material can be attributed to the low density (see the previous subsection) of the pellet. The coupling factor (k_p) of PZT-5A is 0.60, which is comparable to the best value (0.55) of our PNZT pellets with much lower density. The strain coefficient (d_{31}) of PZT-5A is $-171 \times 10^{-6}\,kV^{-1}\,mm$, which is lower than that ($-375 \times 10^{-6}\,kV^{-1}\,mm$) of our PNZT pellets. Thus, inspite of the low density of the pellets of our sol–gel derived materials sintered at a relatively low temperature of 1000 °C, the piezoelectric properties of our material are often comparable to commercially available PZT-5A. This indicates that the powder produced by the present sol–gel technique holds great promise, and, with proper consolidation, might surpass commercial PZT-5A in performance.

4. Conclusions

A new sol–gel method has been developed for preparing Nb-doped PZT powder, using chemicals stable in ambient atmosphere. The powder produced by this method was compacted to pellets by sintering in air for a few hours at 1000 °C. The sintering temperature in the present method was lower than those commonly used in preparing PZT by solid-state reactions. Nb doping increased the rhombohedral distortion in the PZT crystal structure and enhanced piezoelectric properties. The pellets of Nb-doped PZT had maximum values of dielectric constant of 625 and planar coupling coefficient (k_p) of 0.55, which were 27 and 77% higher, respectively, than those of undoped PZT prepared identically by the same sol–gel technique. The strain coefficient (d_{31}) of the Nb-doped pellets was $-375 \times 10^{-6}\,kV^{-1}\,mm$, which was about 15 times that of the undoped PZT pellets. Superior properties of Nb-doped PZT prepared by the present sol–gel route make the present technique attractive.

References

1. B. JAFFE, W. R. COOK Jr and H. JAFFE, "Piezoelectric Ceramics" (Academic Press, New York, 1971) pp. 135–171.
2. S. TROILER-McKINSTRY and R. E. NEWNHAM, *MRS Bull.* **28** (1993) 27.
3. K. UCHINO "Problem Solving Piezoelectric Actuators" (Morikita Publ., Tokyo, 1991).
4. G. HAERTLING, in "Ceramic Materials for Electronics", 2nd Edn, edited by R.C. Buchanan (Marcel Dekker Inc., New York, 1991) p. 129.
5. R. GERSON, *J. Appl. Phys.* **31** (1960) 188.
6. M. YOKOSUKA, T. OCHIAI and M. MARUTAKE, *Jpn. J. Appl. Phys.* **30** (1991) 2228.
7. B. JAFFE, W. R. COOKE Jr and H. JAFFE, "Piezoelectric Ceramics" (Academic Press, New York, 1971) pp. 253–69.
8. R. ROY, *Science* **238** (1987) 1664.
9. K. HIGUCHI, K. MIYAZAWA, T. SAKUMA and K. SUZUKI, *J. Mater. Sci.* **29** (1994) 436.
10. K. AOKI, Y. FUKUDA and A. NISHIMURA, *Jpn. J. Appl. Phys.* **32** (1993) 4147.
11. G. YI, Z. WU and M. SAYER, *J. Appl. Phys.* **64** (1988) 2717.
12. J. S. OBHI and A. PATEL, *Integrated Ferroelectrics* **5** (1994) 155.
13. C. D. E. LAKEMAN and D. A. PAYNE, *J. Amer. Ceram. Soc.* **75** (1992) 3091.
14. C. K. BARLINGAY and S. K. DEY, *Mater. Res. Soc. Symp. Proc.* **224** (1991) 311.
15. A. H. CARIM, B. A. TUTTLE, D. H. DOUGHTY and S. L. MARTINEZ, *J. Amer. Ceram. Soc.* **74** (1991) 1455.
16. P. P. PHULE, *J. Mater. Res.* **8** (1993) 334.
17. IRE Standards on Piezoelectric Crystals: Measurement of Piezoelectric Ceramics, 1961, Proceedings of the IRE (Institute of Radio Engineers, New York, 1961) p. 1161.
18. D. A. BERLINCOURT, D. R. CURRAN and H. JAFFE, in "Physical Acoustics", Vol. 1, Part A, edited by W.P. Mason (Academic Press, New York, 1964) p. 169.
19. J. -P. HAHN and G. KOSTORZ, *Mater. Res. Soc. Symp. Proc.* **243** (1992) 317.
20. Morgan Matroc Inc., Vernitron Division, "Piezoelectric Technology: Data for Designers" (Morgan Matroc Inc., Bedford, Ohio, 1991).
21. J. M. HERBERT, "Ferroelectric Transducers and Sensors" (Gordon and Breach Science Publishers, New York, 1982) pp. 103–124.
22. G. H. HAERTLING, *J. Amer. Ceram. Soc.* **54** (1971) 303.

Received 18 December 1995
and accepted 8 May 1996